

# MEASUREMENT INTEGRATED SIMULATION TO PROVIDE ACCURATE INFORMATION OF BLOOD FLOWS

TOSHIYUKI HAYASE \*

*Institute of Fluid Science, Tohoku University,  
2-1-1 Katahira, Aoba-ku, Sendai 980-8577, Japan*

KENICHI FUNAMOTO

*Institute of Fluid Science, Tohoku University,  
2-1-1 Katahira, Aoba-ku, Sendai 980-8577, Japan*

In order to make an accurate diagnosis in cases of serious cardiovascular diseases such as aortic or cerebral aneurysms, a method to obtain detailed information on the blood flow velocity and pressure is essential, measurement and simulation being the basic tools for this. In this article, a general formulation of measurement integrated simulation is first explained and then the results of numerical experiments for ultrasonic measurement integrated simulation of an aneurysmal aorta and MR measurement integrated simulation of a cerebral artery are presented.

*Keywords:* numerical realization; flow observer; blood flow; aneurysmal aorta; ultrasonic measurement; cerebral artery; MR measurement; flow simulation.

## 1. Introduction

In order to make an accurate diagnosis in cases of serious cardiovascular diseases such as aortic or cerebral aneurysms, a method to obtain detailed information on the blood flow velocity and pressure is essential, measurement and simulation being the basic tools for this.

Among a number of measurement methods, ultrasound color Doppler imaging is widely used since it provides a real-time image of the blood flow structure and vessel configuration non-invasively with relatively compact equipment [1]. However, the velocity measurement with this apparatus provides only the velocity component along the ultrasound beam, and, therefore, it is difficult to comprehend the exact three-dimensional blood velocity field.

As a counterpart of measurement, numerical simulation of the blood flow has been extensively studied. Realistic solutions of the blood velocity and pressure are obtained by solving the fundamental equations of the flow for real

---

\* Toshiyuki Hayase is a Tohoku University Global COE Member.

vessel geometries obtained by visualizing methods such as X-ray computer tomography (CT) or magnetic resonance imaging (MRI) [2,3]. However, the simulation has an inherent problem of difficulty in specifying boundary conditions and/or initial conditions, and the calculated blood flow is similar but not exactly identical to the real one.

In order to overcome shortcomings of measurement and simulation, many studies have been carried out to combine them so as to develop a new methodology. Assimilation is a method commonly used in numerical weather prediction [4]. In a numerical simulation to predict future weather conditions, the initial condition is repeatedly updated at certain time intervals using the latest computational results and the measurement data around the computational grid points. A Similar concept, namely, interactive computational-experimental methodology (ICEME) was proposed by Humphrey et al [5] for application to engineering problems. Zeldin and Meade applied the Tikhonov regularization method, which is common in inverse problems, to obtain an optimum solution to estimate the real flow from the numerical and measurement results [6]. Studies have been made to apply CFD (computational fluid dynamics) schemes to modify PIV (particle imaging velocimetry) measurements to satisfy physical constraints such as the continuity equation [7]. The observer and Kalman filter, which are fundamental tools in modern control theory, have been applied to flow problems [8]. The authors have proposed a concept of numerical realization [9], which is defined as a numerical simulation with a mechanism to include information on real phenomena appropriately. Figure 1 explains the numerical realization based on the concept of the observer in control theory [10]. A finite number of measurable output signals are defined in the real flow as well as in the simulation, and a feedback signal proportional to the difference between the output signals of the measurement and the simulation is added to the simulation to converge to the real flow. This methodology, measurement-integrated (MI) simulation, has been successfully applied to obtain field information for a turbulent flow in a square duct [11] and in a Karman vortex street behind a square cylinder [12].

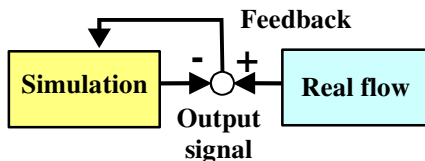


Figure 1. Numerical realization based on flow observer.

For medical application of MI simulation, the authors have proposed ultrasonic-measurement-integrated (UMI) simulation of the blood flow by integrating the ultrasound blood velocity measurement and the numerical simulation based on the flow observer. Since existing theory of observers is not applicable to complex flow problems, design and evaluation of the feedback schemes were made using numerical experiment in various conditions: two-dimensional unsteady problems [13,14] or three-dimensional steady [15] and unsteady problems [16]. Measurement integrated simulation was also applied to magnetic resonance (MR) measurement. A numerical experiment revealed that blood flow in a cerebral artery was successfully reproduced by MR measurement integrated simulation [17].

In this article, a general formulation of the MI simulation is first explained and then the results of numerical experiments for UMI simulation in an aneurysmal aorta and MR measurement integrated simulation in a cerebral artery are presented.

## 2. General Formulation

The dynamic behavior of an incompressible and viscous flow field is governed by the Navier-Stokes equation and a pressure equation derived from the equation of continuity with appropriate initial and the boundary conditions. A discrete model is described as follows:

$$\begin{cases} \frac{d\mathbf{u}_N}{dt} = g_N(\mathbf{u}_N) + h_N(\mathbf{p}_N) + \mathbf{f}_N \\ \Delta_N \mathbf{p}_N = q_N(\mathbf{u}_N) + \nabla_N \mathbf{f}_N \end{cases}, \quad (1)$$

where  $\mathbf{u}_N$  and  $\mathbf{p}_N$  are the  $3N$ -dimensional vector consisting of velocity components at  $N$  grid points and the  $N$ -dimensional vector consisting of pressure divided by the density at  $N$  grid points, respectively.  $\mathbf{f}_N$  is external force which is used as the feedback signal in MI simulation.  $\nabla_N$  and  $\Delta_N$  are matrices to express the discrete model of  $\nabla$  and  $\Delta$ , respectively.  $g_N$ ,  $h_N$ , and  $q_N$  are given as follows.

$$\begin{aligned} g_N(\mathbf{u}_N) &= -(\mathbf{u}_N \cdot \nabla_N) \mathbf{u}_N + \nu \cdot \Delta_N \mathbf{u}_N \\ h_N(\mathbf{p}_N) &= -\nabla_N \mathbf{p}_N \\ q_N(\mathbf{u}_N) &= -\nabla_N \left( (\mathbf{u}_N \cdot \nabla_N) \mathbf{u}_N \right) \end{aligned}, \quad (2)$$

The real flow without external force is described by the following equation:

$$\left\{ \begin{array}{l} \frac{d}{dt} D_N(\mathbf{u}) = D_N(g(\mathbf{u})) + D_N(h(p)) \\ D_N(\Delta p) = D_N(q(\mathbf{u})) \end{array} \right. , \quad (3)$$

where  $D_N$  is the operator to extract the information of the real flow at the computational grid points.

In MI simulation, on the other hand, the external force is applied as the feedback signal denoted by a function of real flow and numerical simulation. In the present study, we consider the case of feedback signal  $\mathbf{f}_N$  denoted by a linear function of the difference of velocity and pressure between real flow and numerical simulation:

$$\mathbf{f}_N \equiv -\mathbf{K}_u \mathbf{C}_u \{ \mathbf{u}_N - D_N(\mathbf{u} + \boldsymbol{\varepsilon}_u) \} - \mathbf{K}_p \mathbf{C}_p \{ \mathbf{p}_N - D_N(\mathbf{p} + \boldsymbol{\varepsilon}_p) \} , \quad (4)$$

where  $\mathbf{K}_u$  and  $\mathbf{K}_p$  denote the  $3N \times 3N$  and  $N \times N$  feedback gain matrices of velocity and pressure, respectively,  $\mathbf{C}_u$  and  $\mathbf{C}_p$  denote the  $3N \times 3N$  and  $N \times N$  diagonal matrices to identify the measurable velocity and pressure data, respectively, and  $\boldsymbol{\varepsilon}_u$  and  $\boldsymbol{\varepsilon}_p$  denote the  $3N$  and  $N$ -dimensional vector of velocity and pressure measurement error, respectively.

### 3. Numerical Experiment of Measurement Integrated Simulation

Results of the numerical experiment are shown in the following for cases: (1) UMI simulation in an aneurysmal aorta [16] and (2) MR measurement integrated simulation in a cerebral artery [17]. Calculation was performed with SGI Prism in the AFI Research Center, Institute of Fluid Science, Tohoku University.

#### 3.1. Ultrasonic Measurement Integrated Simulation in Aneurysmal Aorta

Based on the concept of the flow observer, we have developed Ultrasonic-Measurement-Integrated (UMI) simulation by integrating ultrasonic color Doppler imaging and numerical simulation to reproduce the real blood flow numerically with the aid of feedback [16]. Figure 2 shows a schematic diagram of the UMI simulation. In the UMI simulation, at a number of grid points selected as feedback points in the feedback domain, feedback signals

proportional to the optimal estimation of the difference between the velocity vectors determined by measured and computed Doppler velocities are generated and added to the numerical simulation as artificial force during the computational process.

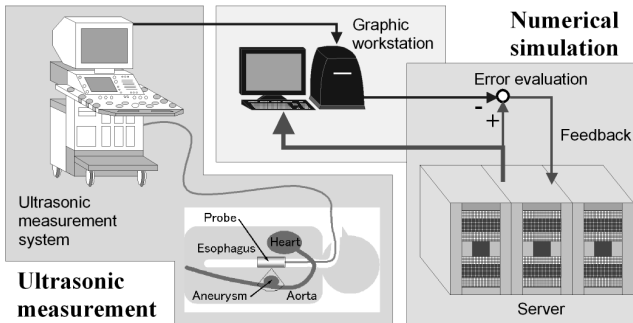


Figure 2. Schematic diagram of UMI simulation system.

In this section, a numerical experiment of UMI simulation of a three-dimensional unsteady blood flow field in an aneurysm was performed to evaluate the effectiveness of UMI simulation for real blood flow. A numerical solution obtained by assuming realistic boundary conditions was first defined as a model of real blood flow (a standard solution), and then UMI simulation was investigated with a focus on the reproduction of the standard solution. In the UMI simulation, a simplified boundary condition that was different from that of the standard solution was applied, and feedback signals were generated by comparing projected velocity information of simulated measurement and computation. In the projection of velocity vectors, a transesophageal ultrasonic measurement of blood flow was assumed in the three-dimensional aneurysmal domain using one probe, which measures only a one-directional velocity component along the ultrasonic beam (Doppler velocity).

The objective flow in this study was the blood flow in an aneurysmal aorta. A 76-year-old female patient, who had no significant complications, with a chronic aortic aneurysm in her descending aorta participated in this study. The cardiac output was  $7.0 \times 10^{-5} \text{ m}^3 \text{ s}^{-1}$  and the heart rate was 1.0 Hz during the measurement. Figure 3(a) shows the full blood vessel configuration reconstructed from the sliced images acquired by X-ray CT (Aquilion<sup>TM</sup> 16, Toshiba, Tokyo, Japan) by means of commercial three dimensional (3D)

reconstruction software (Mimics 7.3, Materialise, Leuven, Belgium). The UMI simulation in this study dealt with the blood flow in a partial domain in the vicinity of the aneurysm as shown in Fig. 3(b). Table 1 summarizes the parameters used in the 3D unsteady blood flow analysis. An orthogonal equidistant computational grid was generated by introducing a staggered grid system with  $N_x \times N_y \times N_z = 43 \times 30 \times 91$  grid points.

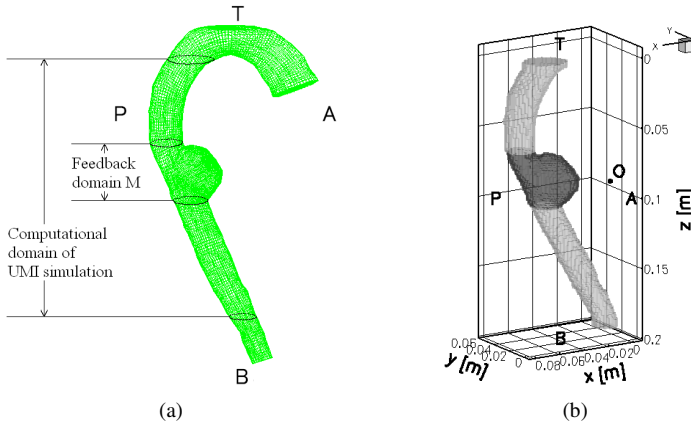


Figure 3. Computational domains of (a) whole aorta with an aneurysm for FLUENT and of the descending aorta with feedback domain M (dark gray zone) and origin O of ultrasonic beam or ultrasound probe position for UMI simulation.

Table 1. Computational conditions for three-dimensional unsteady blood flow analysis.

Heart rate	1.02 Hz
Cardiac cycle $T$	0.98 s
Cardiac output	$7.00 \times 10^{-5} \text{ m}^3/\text{s}$
Entrance flow	$4.90 \times 10^{-5} \text{ m}^3/\text{s}$
Maximum mean velocity $u'_{\max} (U)$	0.37 m/s
Entrance vessel diameter $D(L)$	$29.25 \times 10^{-3} \text{ m}$
Kinematic viscosity $\nu$	$4.0 \times 10^{-6} \text{ m}^2/\text{s}$
Characteristic time $D/u'_{\max}$	0.080 s
Womersley number $D\sqrt{2\pi}/T\nu$	37
Maximum Reynolds number $u'_{\max} \cdot D/\nu$	2700

The space-averaged error norms,  $\bar{e}_M(\mathbf{u}, t)$  and  $\bar{e}_M(p, t)$ , of the velocity vector and the pressure in the aneurysm (feedback domain M) were calculated at each moment as shown in Fig. 4. The ordinary simulation has a relatively large error

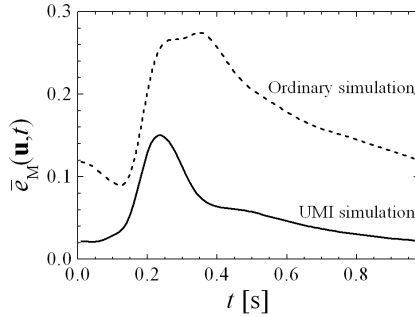


Figure 4. Time-variations of space-averaged error norms of (a) velocity vector and (b) pressure in the aneurysm of the ordinary simulation and in the UMI simulation with ideal feedback at  $Kv^* = 5$ .

in the deceleration phase ( $0.13 \text{ s} \leq t \leq 0.33 \text{ s}$ ). The UMI simulation resulted in smaller error than the ordinary simulation at all phases. The calculation of space-time-averaged error norms,  $\bar{e}_{MT}(\mathbf{u})$  and  $\bar{e}_{MT}(p)$ , of UMI simulation indicates that the application of feedback in feedback domain M using one probe reduced the error in the aneurysm by a factor of 0.31 for the velocity vector in one cardiac cycle.

In order to investigate the effectiveness of UMI simulation for providing information on hemodynamic stress on a blood vessel for advanced medical

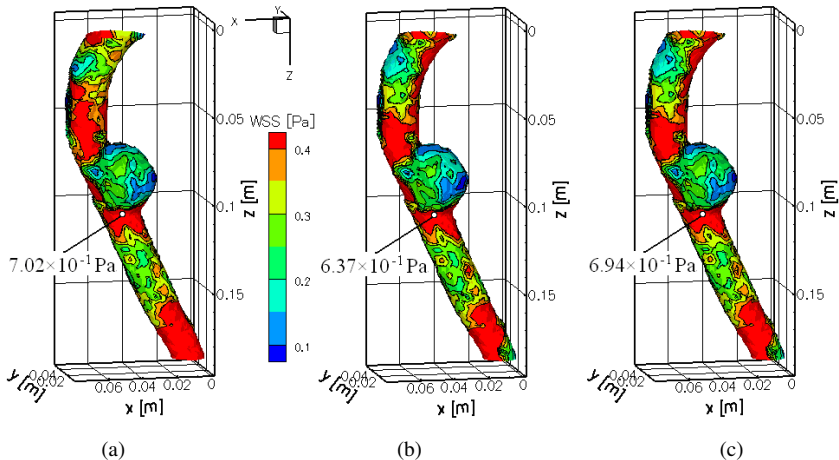


Figure 5. Comparison of time-averaged wall shear stress distribution on the blood vessel between (a) the standard solution, (b) the ordinary simulation, and (c) the UMI simulation with ideal feedback at  $Kv^* = 5$ . Each white dot implies the local maximum value of wall shear stress at the aneurysmal neck.

diagnosis of circulatory diseases, wall shear stress distribution was calculated by first-order numerical differentiation of the velocity vectors. Figure 5 compares the time-averaged wall shear stress distribution between the standard solution, the ordinary simulation and the UMI simulation. All simulations show similar distributions, but the ordinary simulation tends to estimate lower wall shear stress in the aneurysm. The UMI simulation displays a similar distribution as the ordinary simulation in the upstream domain, but accurately provides the wall shear stress distribution of the standard solution in the aneurysm. In Fig. 5, a white dot represents the position of the local maximum value of the time-averaged wall shear stress at the aneurysmal neck.

### 3.2. MR Measurement Integrated Simulation in Cerebral Artery

We have previously proposed magnetic resonance (MR)-measurement-integrated (MR-MI) simulation by integrating MR measurement and numerical simulation [17]. Figure 6 shows a schematic diagram of the system of MR-MI simulation of blood flow. In such simulation, artificial body forces, which are generated by comparing 3D velocity vectors obtained by PC MRI measurement and the corresponding computational results, are added to the numerical simulation. This feedback process is expected to enable reproduction of the real blood flow field computationally by convergence of computational results with those of PC MRI measurement. With this methodology, it is likely that a numerical solution whose resolution is better than the MR measurement can be acquired and that the effect of errors included in the measurement can be eliminated.

In this section, the computational accuracy of the blood flow field and hemodynamic information of the MR-MI simulation with the simplified

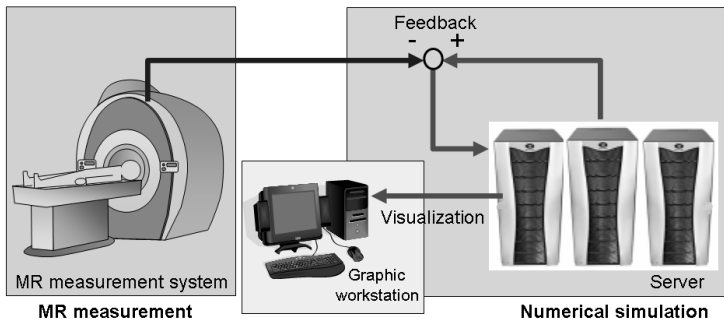


Figure 6. Schematic diagram of MR-measurement-integrated (MR-MI) simulation system.

boundary conditions were investigated by numerical experiments dealing with the reproduction of steady blood flow field in an aneurysm which developed at a bifurcation of a cerebral artery.

We first obtained a standard solution as a model of real blood flow with velocity vectors obtained by PC MRI measurement at the boundaries. MR-MI simulation was then performed using the data of the standard solution, and its ability to reproduce the standard solution was examined. The objective was the blood flow in a cerebral aneurysm at the bifurcation between basilar and superior cerebellar arteries in a 70-year-old female patient. This study was approved by the institutional review board of Hamamatsu University School of Medicine, and informed consent was obtained from the patient.

MR imaging was performed by a 1.5 T MR scanner with a head coil. The PC MRI data, which contain information on the blood vessel configuration and the velocity vector of blood flow, were obtained at 20 phases in one cardiac cycle with a sampling time of  $\Delta t = 0.046$  s. The configuration including the cerebral aneurysm and the parent artery, was reconstructed by means of image data processing software, Flova (Renaissance of Technology Corp., Hamamatsu, Japan), from the PC MRI data. We assumed that the blood vessel was rigid because the deformation was subtle, and we generated several computational grid systems with different resolutions. Compromising between the reproducibility of the blood vessel shape and the computational load, a staggered equidistant grid system with  $N_x \times N_y \times N_z = 30 \times 27 \times 26$  ( $\Delta x = \Delta y = \Delta z = 0.5 \times 10^{-3}$  m) shown in Fig. 7 was chosen. With the same software, one inlet, A, and two outlets, B and C, were determined (see Fig. 7), and the velocity information on the boundaries was exported by linear interpolation.

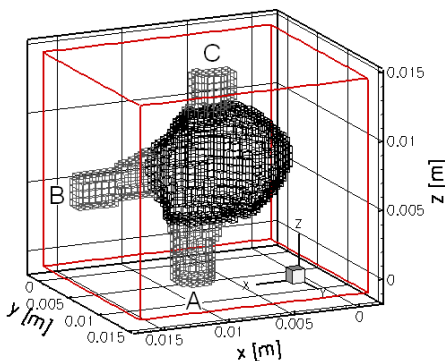


Figure 7. Computational grid (30×27×26) with the feedback domain (black grid lines).

Table 2. Computational conditions.

Entrance flow	$2.68 \times 10^{-6} \text{ m}^3/\text{s}$
Mean velocity $u'_1$	0.23 m/s
Maximum mean velocity $u'_{\max} (U)$	0.42 m/s
Entrance diameter $D(L)$	$4.0 \times 10^{-3} \text{ m}$
Density $\rho$	$1.0 \times 10^3 \text{ kg/m}^3$
Viscosity $\mu$	$4.0 \times 10^{-3} \text{ Pa} \cdot \text{s}$
Maximum Reynolds number $Re_{\max}$	423

For the numerical experiment concerning the reproduction of the steady flow, the first phase in the MR measurement (the initial phase in the systole) was assumed to be steady flow, and a convergent solution obtained with the velocity profiles obtained by PC MRI measurement at boundaries was defined as the standard solution. The mean velocity  $u'_1$  upstream is noted in Table 2.

In the MR-MI simulation, we applied a uniform velocity profile at the upstream boundary and free flow as well as pressure zero conditions at the two downstream boundaries, assuming that the complicated velocity vectors at the boundaries were unknown since the application of the exact velocity profiles is difficult. The computational time increment was set at  $\Delta t = 0.01 \text{ s}$  for the numerical experiment of the reproduction of steady flow.

Figure 8 shows the relationship between  $\bar{e}_M(\mathbf{u}_c, \mathbf{u}_s, t_\infty)$  at  $t = t_\infty$  and the feedback gain. The result of the MR-MI simulation becomes different from that of the ordinary simulation, and the error with respect to the standard solution becomes small due to the feedback. The error monotonically decreases to the minimum value. In this study, the computational accuracy was best improved by setting the feedback gain at  $K_v^* = 3.5$ , which is the approximate value  $K_v^* = 4$  at which the computation diverged. In this case, the error in the velocity field in the blood flow in the cerebral aneurysm was reduced to 13% of that in the ordinary simulation ( $K_v^* = 0$ ).

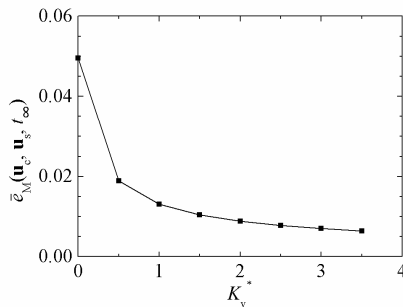


Figure 8. Steady space-averaged error norm of the velocity vector in the aneurysm with the feedback gain.

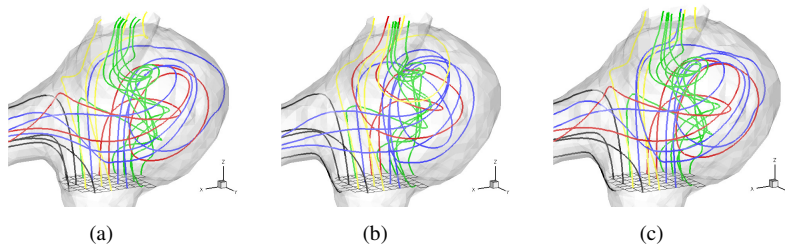


Figure 9. Streamlines departing from the upstream surface of the feedback domain of (a) standard solution, (b) ordinary simulation ( $K_v^* = 0$ ) and (c) MR-MI simulation with  $K_v^* = 3.5$ .

Figure 9 compares the vortex structures in the cerebral aneurysm visualized by the streamlines which depart from multiple points on the first cross section of the feedback domain between the standard solution, the ordinary simulation ( $K_v^* = 0$ ), and the MR-MI simulation with  $K_v^* = 3.5$ . Those different colored streamlines are categorized by their patterns. All results have a  $z$ -directional helical structure (see green streamlines in Fig. 9), which flows from the upstream boundary A to the downstream boundary C, and a swirl in the cerebral aneurysm (see red and blue streamlines). Here, since this result was obtained under the assumption of steady flow, it does not represent the real blood flow field. Though the ordinary simulation (Fig. 9(b)) shows a flow structure similar to the standard solution (Fig. 9(a)), especially for the helical structure, the shapes and positions of the streamlines are different. Several streamlines that swirl in the cerebral aneurysm exit from the opposite outlet compared with those in the standard solution (see red streamlines). In Fig. 9(c), owing to the improvement of the computational accuracy in the cerebral aneurysm by the MR-MI simulation, we can understand the blood flow structure in the cerebral aneurysm of the standard solution more accurately than in the case of the ordinary simulation.

#### 4. Conclusions

In order to accurately diagnose serious cardiovascular diseases such as an aortic or a cerebral aneurysm, a method to obtain detailed information on the blood flow velocity and pressure is essential, measurement and simulation being the basic tools for this. Herein, a general formulation of the measurement integrated simulation was first explained and then the results of numerical experiments for ultrasonic measurement integrated simulation in an aneurysmal aorta and MR measurement integrated simulation in a cerebral artery were presented.

## Acknowledgments

The computer code used in this study was originally developed at the University of California at Berkeley by T. Hayase, J. A. C. Humphrey and R. Greif. The authors acknowledge the support received from the Global Nano-Biomedical Engineering Education and Research Network Centre. The calculations were performed on the integrated supercomputing system in the Advanced Fluid Information Research Center, Institute of Fluid Science, Tohoku University.

## References

1. *Biomedical Engineering Handbook, Second Edition, Volume 1*, edited by J. D. Bronzino, CRC Press (2000).
2. T. W. Taylor and T. Yamaguchi, Three-dimensional simulation of blood flow in an abdominal aortic aneurysm — steady and unsteady flow cases. *J Biomech Eng* **116**, 89–97 (1994).
3. E. S. Di Martino, G. Guadagni, A. Fumero, G. Ballerini, R. Spirito, P. Biglioli and A. Redaelli, Fluid-structure interaction within realistic three-dimensional models of the aneurysmatic aorta as a guidance to assess the risk of rupture of the aneurysm. *Med Eng Phys* **23**, 647–655 (2001).
4. S. G. Benjamin, D. Dévényi, S. S. Weygandt, K. J. Brundage, J. M. Brown, G. A. Grell, D. Kim, B. E. Schwartz, T. G. Smirnova, T. L. Smith and G. S. Manikin, An hourly assimilation-forecast cycle. *The RUC Monthly Weather Review* **132**, 495–518 (2004).
5. J. A. C. Humphrey, R. Devarakonda and N. Queipo, Interactive computational-experimental methodologies (ICEME) for thermofluids research: application to the optimized packaging of heated electronic components. *Computers and Computing in Heat Transfer Science and Engineering*, edited by K. T. Yang and W. Nakayama, CRC Press and Begell House, New York, 293–317 (1993).
6. B. A. Zeldin and A. J. Meade, Jr., Integrating experimental data and mathematical models in simulation of physical systems. *AIAA J* **35**, 1787–1790 (1997).
7. T. Ido, Y. Murai and F. Yamamoto, Postprocessing algorithm for particle-tracking velocity based on ellipsoidal equations. *Experiments in Fluids* **32**, 326–336 (2002).
8. M. Uchiyama and K. Hakomori, Measurement of instantaneous flow rate through estimation of velocity profiles. *IEEE Trans Automat Contr* **AC-28**, 380–388 (1983).
9. T. Hayase, K. Nisugi and A. Shirai, Numerical realization of flow field by integrating computation and measurement. *Proceedings of Fifth World Congress on Computational Mechanics, WCCM V*, Paper-ID: 81524, 1–12 (2002).

10. R. E. Skelton, *Dynamic Systems Control*, John Wiley & sons (1988).
11. T. Hayase and S. Hayashi, State estimator of flow as an integrated computational method with feedback of online experimental measurement. *J Fluids Eng Trans ASME* **119**, 814–822 (1997).
12. K. Nisugi, T. Hayase and A. Shirai, Fundamental study of hybrid wind tunnel integrating numerical simulation and experiment in analysis of flow field. *JSME Int J, Ser. B* **47**, 593–604 (2004).
13. K. Funamoto, T. Hayase, A. Shirai, Y. Saijo and T. Yambe, Fundamental study of ultrasonic-measurement-integrated simulation of real blood flow in the aorta. *Annals Biomed Eng* **33**, 413–426 (2005).
14. K. Funamoto, T. Hayase, Y. Saijo and T. Yambe, Detection and correction of aliasing in ultrasonic measurement of blood flows with ultrasonic-measurement-integrated simulation. *Tech Health Care* **13**, 331–344 (2005).
15. K. Funamoto, T. Hayase, Y. Saijo and T. Yambe, Numerical experiment of transient and steady characteristics of ultrasonic-measurement-integrated simulation in three-dimensional blood flow analysis. *Annals Biomed Eng* (submitted).
16. K. Funamoto, T. Hayase, Y. Saijo and T. Yambe, Numerical experiment for ultrasonic-measurement-integrated simulation of three-dimensional unsteady blood flow. *Annals Biomed Eng* **36**, 1383–1397 (2008).
17. K. Funamoto, Y. Suzuki, T. Hayase, T. Kosugi and H. Isoda, Numerical validation of MR-measurement-integrated simulation of blood flow in a cerebral aneurysm. *Annals Biomed Eng* (submitted).